Recent advances in 3D SEM surface reconstruction

Ahmad P. Tafti [a,*], Andrew B. Kirkpatrick [b], Zahrasadat Alavi [c], Heather A. Owen [b], Zeyun Yu [a,*]

[a] Department of Computer Science, University of Wisconsin-Milwaukee, Milwaukee, WI 53211, USA
[b] Department of Biological Sciences, University of Wisconsin-Milwaukee, Milwaukee, WI 53211, USA
[c] Department of Electrical Engineering, University of Wisconsin-Milwaukee, Milwaukee, WI 53211, USA

ARTICLE INFO

ABSTRACT

The scanning electron microscope (SEM), as one of the most commonly used instruments in biology and material sciences, employs electrons instead of light to determine the surface properties of specimens. However, the SEM micrographs still remain 2D images. To effectively measure and visualize the surface attributes, we need to restore the 3D shape model from the SEM images. 3D surface reconstruction is a longstanding topic in microscopy vision as it offers quantitative and visual information for a variety of applications consisting medicine, pharmacology, chemistry, and mechanics. In this paper, we attempt to explain the expanding body of the work in this area, including a discussion of recent techniques and algorithms. With the present work, we also enhance the reliability, accuracy, and speed of 3D SEM surface reconstruction by designing and developing an optimized multi-view framework. We then consider several real-world experiments as well as synthetic data to examine the qualitative and quantitative attributes of our proposed framework. Furthermore, we present a taxonomy of 3D SEM surface reconstruction approaches and address several challenging issues as part of our future work.

© 2015 Elsevier Ltd. All rights reserved.

1. Introduction

3D visualization from a set of 2D images has been an operational research topic over the last 20 years. The research has found a broad range of applications including 3D world scene reconstruction, movie making, medical visualization, virtual tourism, mobile robot navigation, virtual reality, and computer aided design (Agarwal et al., 2011; Cyganek and Siebert, 2009; Hartely and Zisserman, 2004; Li et al., 2012; Lourakis and Argyros, 2009; Samak et al., 2007; Snavely et al., 2008; Wohler, 2013). The technique of scanning electron microscope (SEM) imaging has also been traditionally employed in a variety of areas to "view" the surface structure of microscopic samples (Bogner et al., 2007; Bozzola and Russel, 1992; Cazaux, 2005; Chandler and Robertson, 2009; Egerton, 2005; Parry-Vernon, 2000; Rittscher et al., 2008), providing 2D images to examine and interpret the surface properties of micro objects. Producing 3D shapes from SEM micrographs would provide true anatomic surfaces which definitely allow for quantitative measurements and informative visualization of the systems being investigated. Many facets of science could benefit from 3D

SEM surface reconstruction techniques. For instance, biological researchers can get 3D surface models of specimens to investigate their surface characteristics, such as recognizing roughness, flatness, and waviness. Medical researchers are interested in 3D modeling to inspect cell anatomy, taking advantages of virtual reality applications in medicine (Rittscher et al., 2008). There are also a bunch of aims for material science and mechanical engineering in which 3D representation of material properties is critical to accurately measure a fractal dimension and surface roughness, designing a micro article which needs to fit into a tiny appliance (Samak et al., 2007; Chen et al., 2012; Cornille et al., 2003; Raspanti et al., 2005).

1.1. SEM imaging

In electron microscopy, the source of illumination of the specimen comes from a beam of electrons (Chandler and Robertson, 2009). The beam is generated in a vacuum by an object called an "electron gun". The basic construction of the electron gun comprises three key elements; a filament, a shield, and an anode. The filament serves as the source of electrons for the beam. Filaments can vary in composition from tungsten to lanthanum hexaboride (Parry-Vernon, 2000). The second component is the shield. The shield, also referred to as Wehnelt cylinder, bias shield, focusing

electrode and grip cap, primarily functions to direct the emitted electrons in a downward trajectory in the column of the microscope. The final component is the anode. The disc like structure is located directly underneath the shield and aids in drawing electrons down into the column at a constant speed (Bogner et al., 2007). The electrons emitted from the gun are controlled by several electromagnetic lenses placed at various points within the column of the microscope. These lenses control the coherency of the beam, correct for spherical aberration and regulate spot size. In addition, SEMs exhibit an extra pair of coils called deflection coils, located near the final lens of the column. During the scanning operation, voltage passing through the coils is oscillated. This produces a magnetic field which influences the electron beam, causing it to move back and forth, or rastor, across the specimen (Chandler and Robertson, 2009).

As the beam is rastored, the electrons from the beam will interact with those residing at the surface of the sample. The interaction will subsequently yield two types of signal. One form of signal involves the electrons from the beam that collide with the sample and change trajectory without losing significant energy or momentum. These electrons are called elastically backscattered electrons (BSE). The detection of BSE signal has proven beneficial to compositional studies of unknown and synthesized materials. Commonly, greater atomic number of the element within a sample, the greater likelihood of generating BSE (Chandler and Robertson, 2009). This relationship can be used to provide compositional information of a sample as elements with a greater atomic number will produce more BSE and a greater signal (Parry-Vernon, 2000). However, due to the high energy with which these electrons interact with the sample, it is possible for these electrons to conduct multiple collisions before escaping, as well as penetrate into the interior of the sample. These particular outcomes result in an excess of signal which negatively influences surface imaging through a reduction of resolution (Chandler and Robertson, 2009). The other product is referred to as secondary electrons (SE). SE result from an inelastic collision between electrons of the beam and the sample. This transfer of energy can cause the sample to eject electrons of significantly lower energy levels BSE or those comprising the beam (Egerton, 2005; Parry-Vernon, 2000). Due to the weak nature of the SE, only those produced at or near the surface are capable of escaping from the sample and producing a detectable signal (Bogner et al., 2007; Bozzola and Russel, 1992; Chandler and Robertson, 2009). It is for this reason that SE images have a higher resolution and greater topological contrast than images produced from BSE as seen in Fig. 1.

With the advent of electron microscopy, novel ways to acquire specimens that were agreeable with the new technology were subsequently investigated. Among biologists, this means preserving the native structure of the sample without compromising the integrity of the vacuum or emission of electrons. Thus the vast majority of biological samples require a consistent methodology for preparation to be viewed by SEM. A generalized protocol for biological specimen preparation is as follows (Chandler and Robertson, 2009): (1) fixation, (2) rinse, (3) post-fixation, (4) rinse, (5) dehydration, (6) critical point drying, (7) specimen mounting, and (8) specimen coating.

To restore the 3D surface model of an object, we need to specify the mutual orientation and location of its images. In a SEM, we can only define the rotation angle manually. It is also necessary to know exactly the rotation axis along the rotation angle. A SEM does not provide rotation axis, and also translation as standard and predefined rules.

1.2. Taxonomy of 3D SEM surface reconstruction

The process of creating a 3D shape model of a microscopic sample is still rather difficult to solve since its three dimensional shape in the real world is only projected into and available as 2D digital images. Over the past few years, there has been an expansion in designing and developing 3D surface reconstruction algorithms for images obtained by a SEM. All these algorithms are categorized into three main classes: (1) single-view (Argyriou and Petrou, 2006; Carli et al., 2011; Drzazga et al., 2006; Ikeuchi and Horn, 1981; Liu et al., 2012; Paluszynski and Slowko, 2005; Pintus et al., 2006; Slowko and Krysztof, 2013), (2) multi-view (Samak et al., 2007; Raspanti et al., 2005; Zolotukhin et al., 2013), and (3) hybrid (Danzl and Scherer, 2003).

There have also been some sorts of 3D SEM volume reconstruction including focused ion beam scanning electron microscopy (FIB-SEM) and electron tomography (ET) (Fridman et al., 2012; Kizilyaprak et al., 2014) in which they have tried to characterize the complex microstructure of a sample in the context of the whole. Using FIB-SEM or ET, a 3D volume of the object or sample is obtained through the acquisition and manipulation of a series of 2D projections (Fridman et al., 2012). The series of images are obtained over a range of directions and orientations. The point is that sample sectioning and possible destruction required by these techniques but not in the 3D SEM surface reconstruction. In the current work, we only explore the use of 3D surface reconstruction techniques for SEM images. Fig. 2 shows a taxonomy of 3D
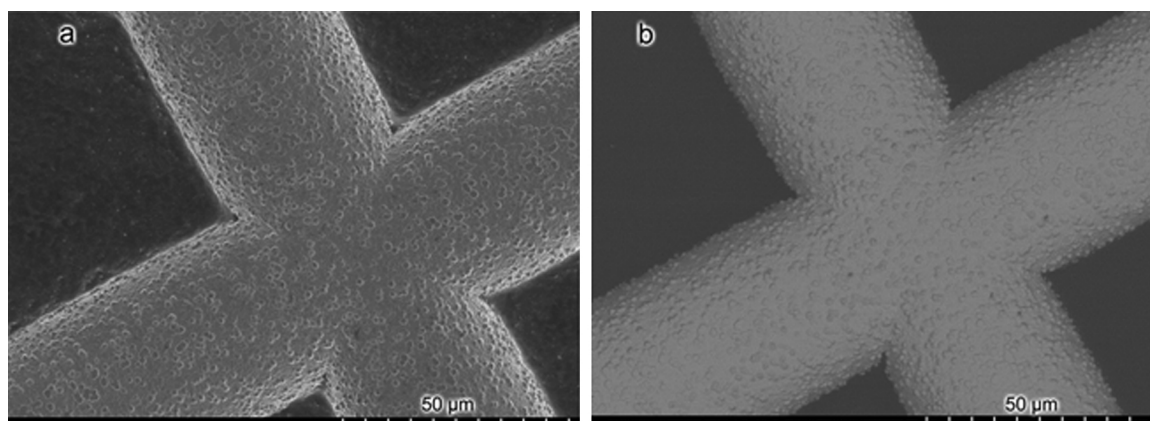

Fig. 1. Secondary electron (SE) and backscatter electron (BSE) micrographs of a copper TEM grid. SE micrograph (a) exhibits greater resolution and topography on the surface of the grid as well as in background. It also provides darker intensities comparing with BSE images. BSE micrograph (b) exhibits greater contrast and brightness between materials comprising the sample. Resolution compared to SE micrograph is much reduced.
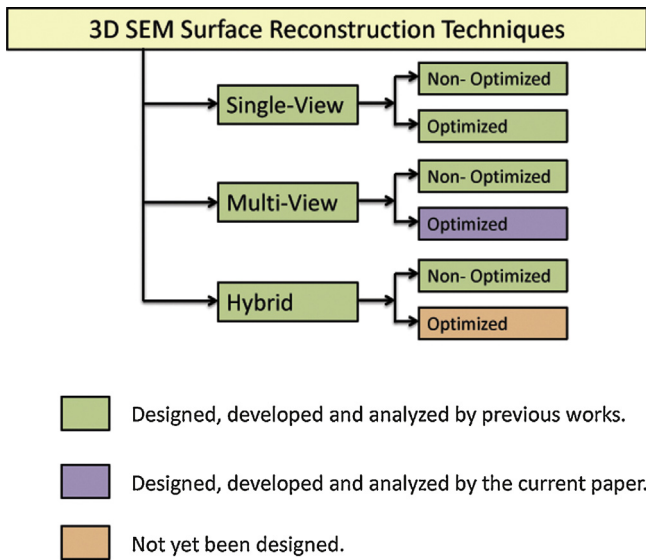
Fig. 2. Taxonomy of 3D SEM surface reconstruction studies.

SEM surface reconstruction studies and highlights our scope in this contribution.

In the following, we reflect the current knowledge and progress in 3D SEM reconstruction of surfaces from 2D images. In the single-view approach, a set of 2D images from a single view point with varying light directions are considered for 3D SEM surface reconstruction. Photometric stereo (PS) is the main algorithm used in this class to produce 3D geometry information of a microscopic sample (Woodham, 1980). PS is a 3D computer vision algorithm which rapidly computes the three dimensional geometry of an object by examining 2D images being viewed from the same viewpoint, same pose, but being illuminated from different directions. The PS method has five general steps: (1) take a set of single view digital images of an object (sample) under the different light directions, (2) determine the light directions, (3) calculate surface normals, (4) calculate albedo, and (5) depth estimation (Woodham, 1980; Hayakawa, 1994). Fundamental basics on PS algorithm can be found in Longuet-Higgins (1981), Warren (2007).

For application of the PS method to scanning electron microscopy, several methods of implementation and instrumentation have been developed and utilized to improve the algorithm and make it more applicable to different areas of research and industry. In 2005, Paluszynski and Slowko (2005) developed a method of PS by applying signal processing methods and shape from shading to reconstruct the third dimension of smooth objects. This method assumes the SE and BSE detectors distributed based on the Lambert's Law distribution (Warren, 2007). Since some instruments utilize only two detectors, this algorithm would not be useful for them. In 2006, Drzazga et al. (2006) developed a method of 3D surface reconstructions of SEM images. This method employed signal processing to eliminate the errors (i.e. distortions) such that the inspection of geometric issues in the micro structures is more feasible.

In 2006, Pintus et al. (2006) proposed and tested a method for automatic alignment of PS performed via a BSE detector. This was proposed since PS is beneficial when sequential acquisition of the backscattered images is performed. This alignment in a SEM was completely controlled by computer, and the authors demonstrated the pixel precision of the reconstructed surface by using the PS method. In 2008, Argyriou and Petrou (2006) developed an iterative PS algorithm in case of multiple highlights and shadows. This algorithm was designed to work with at least three different light sources, and was capable of recognizing unreliable sources based on unreliable pixel intensities. While most of the work has focused on 3D SEM surface reconstruction algorithms, less efforts have been spent on the effects of SEM variables and measurement parameters on 3D reconstruction accuracy. In 2008, Marinello et al. (2008) investigated how SEM instrumental parameters influence the quality of 3D surface reconstruction, recognizing two main classes of various instrument and measuring factors. Their evaluations involved the operation of the most famous commercial software package for SEM surface reconstruction namely Alicona MeX (Mex software, 2005). Image quality and its spatial resolution, magnification, relative position of detectors and tilt angle are among the most important parameters which affect the accuracy of 3D SEM surface reconstruction.

In 2013, Slowko and Krysztof (2013) carried out 3D surface reconstruction for images obtained by a SEM. This method was different in equipment, since it provided the environmental condition of vacuum where a vacuum-detector contained an intermediate vacuum chamber inside which there was a semiconductor BSE detector.

There are also some optimized versions of single-view methods by doing a refinement process in which both SEM parameters and 3D geometry information are optimized simultaneously. In 2005, Kodama et al. (2005) used genetic algorithm to solve the optimization problem employed in surface reconstruction of 2D images obtained from BE and BSE detectors in SEM systems. In this work, it was assumed that the specimen was only inclined to one line scan direction. Thus, for more applicability a number of string coding alternatives were examined to map finite length strings onto 3D surfaces, and finally, representation by a set of coordinates of vertices was selected. The Delaunay triangulation (Okabe et al., 2000) was used for the coding. Since employing genetic algorithm was computationally expensive, hybrid algorithms were used taking advantage of genetic algorithm and simulated annealing algorithm (Kirkpatrick et al., 1983).

In 2007, Yuniarti (2007) solved the PS problem in case of noisy images as inputs of surface reconstruction algorithm. The noisy images make the problem require nonlinear optimization tools. To solve the nonlinear optimization problem the 2D leap frog algorithm (Kozera et al., 2006; Kozera and Noakes, 1999) was employed which converts one problem into a number of smaller optimization problems. In this work, the effect of changing the size of the snapshots on the reconstruction algorithm was analyzed, and eventually was concluded that the larger snapshots improved the quality of the reconstructions, although the computation time would increase. Also, for the purpose of decreasing the number of outliers, median filters were applied to the recovered surface. In 2010, Vynnyk et al. (2010) implemented the PS technique focusing on the detector efficiency and the distribution of the electron beams based on cosine Lambert's law (Warren, 2007). The Cosine Lambert's Law is one of the requirements of the PS technique which was suppressed in this approach. As a result of employing this method, a high lateral and vertical resolution was obtained measuring the structures. One of the main disadvantages of this method is that it is only capable of measuring samples with slope of up to 45 degrees; for larger angles the setup needs to be improved by optimizing the field distribution to which the sample is subjected. In this work, the atomic force microscope was employed for the measurements as well as SEM. This microscope does not damage the surface as others which cannot be used for measuring topography data. The PS algorithm has found its application as a new tool in the semiconductor industry. One of these applications is monitoring manufacturing process precisely to increase the quality of the printed circuits. In 2013, Estellers et al. (2014) used PS method to implement the 3D surface reconstruction of images of printed circuits taken with SEM. This was done to compare the circuit details with the expected circuit which led also to a

deformation field. This enabled the development of an optimization based surface reconstruction algorithm. The results showed robustness to noise and could be applied in the chip manufacturing industry to improve the precision of the lithographic process.

In the multi-view approach, a 3D computer vision algorithm is employed, namely structure from motion (SFM) (Hartely and Zisserman, 2004; Tomasi and Kanade, 1990). This method utilizes stereo pairs taken by tilting the micro object between photographs. SFM is established on the theory of projective geometry, with considering different perspectives from different view angles to restore the 3D structure of a specific object (Hartely and Zisserman, 2004). By using corresponding feature points in image pairs, a 3D point can be reconstructed by triangulation (Hartely and Zisserman, 2004). Basic requirements are the determination of camera calibration (intrinsic camera parameters) and pose (camera rotation and translation), which may be given by a 3*4 camera projection matrix. The projective geometry method allows the projection matrix and 3D points to be estimated using only corresponding points in different views. The SFM method has five major steps (Hartely and Zisserman, 2004; Wohler, 2013; Tomasi and Kanade, 1990): (1) take a set of digital images of an object (sample), (2) identify key points in the images that can possibly be detected in other images in the set, (3) search for corresponding points in images (this step is also called point-matching), (4) use the projection geometry theory to estimate camera projection matrices, and (5) compute 3D surface model using linear triangulation. Further details for SFM algorithm can be found in Hartely and Zisserman (2004).

In 2005, Raspanti et al. (2005) presented a high resolution 3D reconstruction method based on the SFM algorithm. They firstly read a stereo pair of SEM images, then selected on the first picture a user defined number of prominent feature points. They also used Delaunay triangulation (Okabe et al., 2000) to restore the spatial model of a micro sample. In 2007, Samak et al. (2007) used SFM algorithm to reconstruct 3D microstructure surfaces from SEM images. The proposed method first computed 3D points from 2D matched key points, then triangulated the 3D points into the 3D mesh and finally mapped a 2D image as a texture on the shape model.

In 2011, Carli et al. (2011) performed a theoretical uncertainty evaluation of stereo-pairs technique for 3D SEM surface reconstruction. Their work discussed 3D SEM surface reconstruction based on the Piazzesi model function applied to both stereo-pairs and multi-pairs matched through a rank-area-based method. Uncertainty tables have been presented for the different cases of tilt and rotation in a SEM pixel size and rotation angle are areas with the greatest degree of uncertainty in 3D SEM stereo-pairs surface reconstruction. In 2013, Zolotukhin et al. (2013) examined the advantages and limitations of the structure from motion approach to perform 3D reconstruction for SEM images. It was concluded that the algorithm is applicable to build a 3D model of a micro object. Their proposed traditional SFM algorithm received two images from two camera angles, found the correspondence key points, estimated the mutual positions of the images using RANSAC algorithm (Hartely and Zisserman, 2004; Fischler and Bolles, 1981), and built a 3D surface. They did not mention that we may have some invaluable information about SEM camera calibration which is useful to increase the accuracy of the algorithm and reduce the processing time. For example, we have all intrinsic parameters of a SEM, including focal length, principal point coordinate and horizontal and vertical resolution.

The third class of 3D SEM surface reconstruction algorithms called the hybrid method and it offers a compromise between the single-view and the multi-view approaches. In 2003, Danzl and Scherer (2003) presented an algorithm to reconstruct surfaces and 3D images by applying stereo and shading information from two 2D images. The stereo and shading information are complementary

Table 1
Advantages, disadvantages and limitations of 3D SEM surface reconstruction approaches.

Approach	Single-view
Pros	It only requires additional lighting
	It can be easily implemented at an appropriate computational cost
Cons	It is not able to create a whole 3D model since it only uses a single perspective
	The obtained 3D models would be limited to only a particular view angle
	Using standard SEM machines make it difficult to produce images under different illumination directions
Approach	Multi-view
Pros	It can produce a better 3D model since it uses multiple images
	Most SEM machines are able to produce multiple images by tilting the specimen over different angles
Cons	It requires more sophisticated algorithms and computational time
Approach	Hybrid
Pros	It takes advantages of both single-view and multi-view approaches to reconstruct a 3D model
Cons	It is not operational or cost effective with common SEM machines

requirements of the reconstruction, since shape from shading does the reconstruction very well when the 2D data has homogeneous texture and shape from stereo helps when there are various features in the data. Despite previous works which assumed the reflectance map known or given by simple mathematical functions, their work estimated the reflectance map by using a fitting polynomial of degree 4 and used the stereo and shading information simultaneously. The latter was an optimization problem where it minimized an energy function with constraints on shading, height and surface smoothness. This algorithm was run on both synthetic and real SEM data.

We briefly summarize the advantages, disadvantages and limitations of each 3D SEM surface reconstruction approach in Table 1.

Based on the pros and cons of each 3D SEM surface reconstruction method illustrated in Table 1, in this paper, we will enhance the accuracy, reliability, and speed of 3D SEM surface reconstruction by a novel optimized algorithm utilizing the multi-view technique. As we presented in the taxonomy (Fig. 1), an optimized multi-view class of 3D SEM surface reconstruction has not yet been implemented, and it is a major part of our contributions. With the current paper, we design and develop a global optimization framework based on a differential evolutionary (DE) technique (Chakraborty, 2008; Feoktistov, 2006) to restore the 3D surface model of SEM images in a fast and reliable manner. Our proposed framework is also able to calibrate SEM extrinsic parameters in an accurate fashion. The proposed optimized multi-view framework for SEM extrinsic calibration and its surface reconstruction comes in Section 2.

1.3. Generic 3D surface reconstruction

3D surface reconstruction techniques constitute an important part of 3D computer vision. 3D computer vision, also called human-like computer vision, is the ability of using double camera processor devices to take real-time photos of a 3D real-world scene (Cyganek and Siebert, 2009; Lazaros et al., 2008). It compromises the construction of integrated vision systems to realistic problems existing in real world. 3D surface reconstruction has often been used in the process of creating 3D shape models from only a set of 2D images (Cyganek and Siebert, 2009; Hartely and Zisserman, 2004). 3D computer vision has provided an excellent ability to restore the 3D geometry information of a real scene by solving the inversion problem going from 2D to 3D. We list supreme applications of 3D surface

Table 2
The popular applications of 3D surface reconstruction in industry, medicine, and entertainment.

Biomedical and medical	Industrial and commercial
3D microscopy vision	3D representation of mechanical models
3D modeling of tissues	3D representation of material properties
3D tracking of human body parts	Measurement of fractal dimension
Inspection of surfaces	Pose refinement, and height evaluation
Medical visualization	CAD/CAM, game, and animation
Remote surgery	Roughness measurement
3D modeling of cells	Mobile robot navigation
Biomedicine and medicine virtual reality	Virtual city and virtual museum

reconstruction into two categories as shown in Table 2 (Agarwal et al., 2011; Cyganek and Siebert, 2009; Hartely and Zisserman, 2004; Li et al., 2012; Lourakis and Argyros, 2009; Samak et al., 2007; Wohler, 2013; Rittscher et al., 2008; Cornille et al., 2003; Lazaros et al., 2008).

The origin of 3D computer vision dates back to 1957 where Gilbert Hobrough illustrated a method and designed an apparatus to analog implementation of stereo image correlation (Hobrough, 1957). In 1963, Larry Roberts proposed the first 3D surface reconstruction technique by developing a machine perception algorithm which could create and display 3D geometry information of objects from a single 2D photo (Roberts, 1963). Then, in 1970, B.K.P. Horn designed another 3D surface reconstruction technique called shape-from-shading (SFS) (Horn, 2012). SFS used shading from an individual image in order to calculate the surface orientation. R.J. Woodham in 1977, designed the photometric stereo (PS) algorithm (Woodham, 1980) as a multi-view version of shape-from-shading. In 1990, C. Tomasi and T. Kanade were able to estimate 3D surface structure from a sequence of 2D images (Tomasi and Kanade, 1990). They proposed a method called structure from motion (SFM). In 2002, T. Zickler, P.N. Belhumeur, and D. Kriegman designed Helmholtz stereopsis (Zickler et al., 2002) to reconstruct the 3D geometry of an object from a collection of 2D images. In 2011, Shotton et al. (2011) provided a new method to predict 3D positions of body joints from a single depth image in a fast and accurate manner by recording the shape of the reflected points of light by means of a camera. Instead of temporal information, this was known as structured light (or light coding) capture. This technique has famously been used in Microsoft's Kinect accessory. Readers interested in 3D computer vision and 3D surface reconstruction are referred to Cyganek and Siebert (2009), Hartely and Zisserman (2004), Wohler (2013) for further information.

1.4. Motivations and contributions

The motivations of the work are to revisit the state of the art in 3D SEM surface reconstruction techniques to provide a better understanding of the current technologies and discuss possible enhancements in this challenging application to fulfill the following objectives: (1) bringing advanced 3D technology to the SEM community, and creating realistic anatomic shapes from microscopic samples; (2) allowing rotation and depth estimations for further interpretation of microscopic objects, and providing quantitative and visual information; and (3) identifying the grant challenges in 3D SEM surface reconstruction, planning several interesting directions for 3D microscopy vision and drawing attention from the 3D computer vision community to the fast-growing SEM application area.

We briefly summarize our Main contributions in the following:

- We review the evolution of 3D SEM surface reconstruction systems, and discuss the success and failure of existing approaches to the problem. We explain the state of the art algorithms adopted over the years in attempting to solve the 3D surface reconstruction from SEM images. The present paper is expected to highlight the important roles and applications of 3D computer vision algorithms in the area of 3D microscopy vision, particularly 3D surface reconstruction from SEM images.
- We present a taxonomy of nearly 23 models, which provides a critical comparison of the current approaches, their capabilities, and deficiencies and conclude with some of the challenges that can be resolved with recent advances in 3D computer vision. We do hope that this work will serve as a guide for 3D SEM surface reconstruction.
- With the current work, we novel design and develop an optimized multi-view framework to calibrate SEM extrinsic parameters and restore the 3D shape model in a fast, reliable, and accurate fashion. Our work is the first which designs and examines a new optimized technique to make a 3D shape model from multi-view SEM images.
- As an interesting contribution, this work provides insights and tendencies, and plans several future enhancements to advance the level of the progress and impact of the research area.

The proposed optimized multi-view framework for 3D SEM surface reconstruction is described in Section 2. We then analyze, examine and evaluate our proposed system in Section 3. Discussion including limitations, challenges, and possible future enhancements are presented in Section 4.

2. An optimized multi-view framework for 3D SEM surface reconstruction

In this section, we design and develop an optimized multi-view framework to tackle the problem of 3D surface reconstruction from SEM images. The major part of our work is doing an optimization process by defining a cost function for any set of parameters (3D points and relative poses including extrinsic SEM parameters which specify rotation and translation from one view point to the other). Hence, parameterization of rotation and translation space is the most important part of the work. We first estimate the rotation and translation from the set of corresponding points between two images in the image set (Lowe, 2004; Bay et al., 2008; Calonder et al., 2010; Rublee, 2011). For this purpose we employ the highly used SIFT (Lowe, 2004; Zhao, 2011; Tafti et al., 2015a,b) algorithm along with KNN (Altman, 1992) to find the matching points in the image pair. We examined BRIEF (Calonder et al., 2010), SIFT (Lowe, 2004; Tafti et al., 2015a), and SURF (Bay et al., 2006) feature detectors and eventually chose the SIFT algorithm base on our experiments. Then, we apply an iterative strategy called RANSAC (Hartely and Zisserman, 2004; Fischler and Bolles, 1981) to select the correct inlier points in the set of all corresponding points. A key assumption is that a set of matching points usually consists two types of corresponding points: inliers (correct matching points) and outliers (incorrect matching points). RANSAC algorithm (Hartely and Zisserman, 2004; Fischler and Bolles, 1981) will assist us to find out the inliers. We next take advantages of epipolar geometry (projective geometry) to estimate the rotation and translation, and perform linear triangulation (Hartely and Zisserman, 2004) to initialize the 3D locations of all matching points. The last step is a refinement process by defining a cost function for any set of parameters as to whether this is a good or bad set. Fig. 3 shows the pipeline of our proposed system.
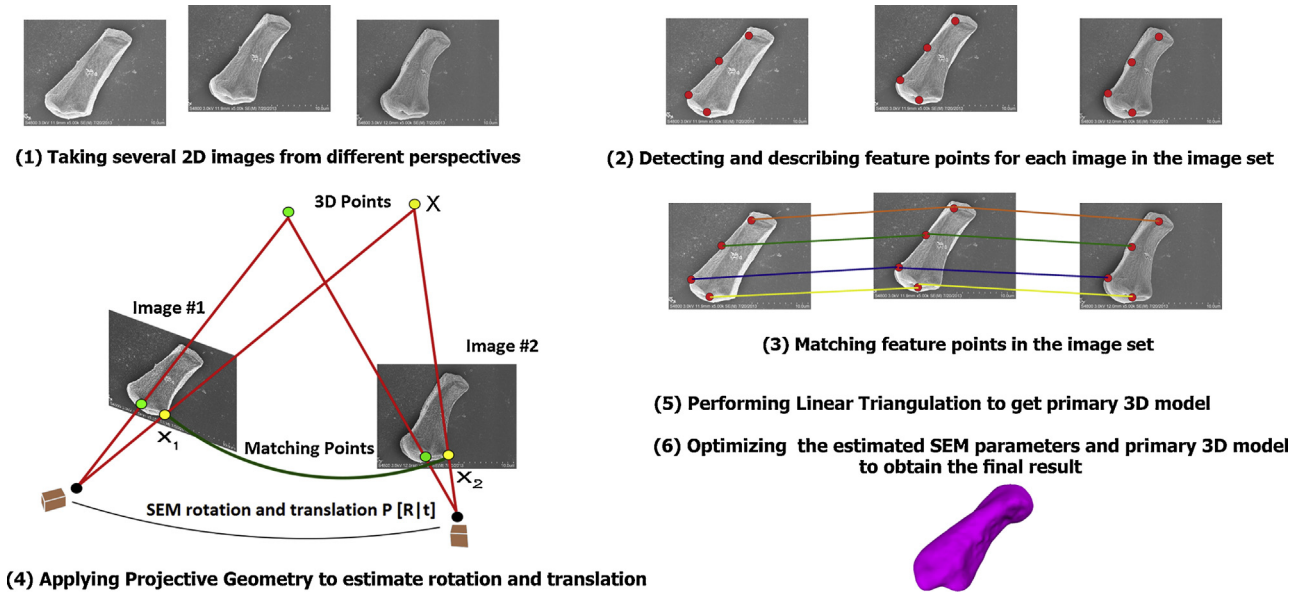
(1) Taking several 2D images from different perspectives

(2) Detecting and describing feature points for each image in the image set

(3) Matching feature points in the image set

(5) Performing Linear Triangulation to get primary 3D model

(6) Optimizing the estimated SEM parameters and primary 3D model to obtain the final result

(4) Applying Projective Geometry to estimate rotation and translation

Fig. 3. The pipeline of our proposed framework includes six different steps. At the first stage, we take several 2D images by tilting the specimen across different angles. This step concerns SEM imaging styles such as tilting the specimen, magnification, and using SE and/or BSE detectors. We then find the feature points in every 2D image and estimate the image motion from a set of matching points. After estimating the relative position of the images, the 3D location of all matching points can be reconstructed by linear triangulation. The latter stage is doing a refinement process by defining a cost function for any set of parameters (3D points and SEM extrinsic parameters) as to whether this is a good or bad set and find the best fitness in the set.

For the refinement, the most important part is to parameterize the space of rotation and translation. In order to have much simplicity and better flexibility, the quaternion parameterization (Hartely and Zisserman, 2004) is applied to formulate the 3D rotation.

A quaternion $\mathbf{z} = a + bi + cj + dk$, where a, b, c, d are real numbers and $i^2 = j^2 = k^2 = -1$, and $\mathbf{z}$ is a unit quaternion if and only if (Hartely and Zisserman, 2004):

$$|z| = \sqrt{a^2 + b^2 + c^2 + d^2} = 1 \tag{1}$$

Then the rotation matrix representation is as follows (Hartely and Zisserman, 2004):

$$R(z) = \begin{vmatrix} a^2 + b^2 - c^2 - d^2 & 2bc - 2ad & 2bd + 2ac \\ 2bc + 2ad & a^2 - b^2 + c^2 - d^2 & 2cd - 2ab \\ 2bd - 2ac & 2cd + 2ab & a^2 - b^2 - c^2 + d^2 \end{vmatrix} \tag{2}$$

We define the translation vector of the second position with respect to the first one as $t = (t_x, t_y, t_z)^\top$. By considering Eq. (2) for rotation parameterization and t for translation, then the parameterization of two projection matrices will be determined by a seven-dimensional vector $\theta = (a, b, c, d, t_x, t_y, t_z)^\top$. Now, SEM extrinsic calibration is equivalent to determining the parameter vector θ^* as in Eq. (3). In this equation, P is the SEM projection matrix which encapsulates rotation and translation (take a look at step (4) in Fig. 3).

$$\theta^* = \arg\min_{\psi}\left(\sum_{i=1}^{N} \|x_1^i - P(X_i)\|^2 + \|x_2^i - P(\psi, X_i)\|^2\right) \tag{3}$$

In generic 3D surface reconstruction, the iterative bundle adjustment algorithms (Lourakis and Argyros, 2009) were frequently employed to solve this kind of equation. The bundle adjustment algorithms are among local minimizer (not global) techniques which suffer from different problems. For instance, they commonly work on differential functions only and it is important to have an initial guess close to the real answer to converge (Rousseeuw, 1984; Torr, 2002; Crandall et al., 2011). In contrast to the traditional bundle adjustment approaches, the differential evolutionary (DE) algorithm (Chakraborty, 2008; Feoktistov, 2006) is a global, population-based, and stochastic optimization strategy which does not tolerate these limitations and also is known as a fast and mighty evolutionary algorithms to optimize real number functions (Ghosh et al., 2014; Nyirarugira and Taeyong, 2013). DE as a genetic searching based minimization algorithm uses generated populations within the parameter space. It first generates an initial population randomly, then iteratively updates them to estimate the best possible values for an optimization problem. The initial population is modified from one generation to the other by using two major operators: (1) mutation and (2) crossover (Chakraborty, 2008; Feoktistov, 2006). The population generation process will be continued until a termination condition is met (i.e. number of generations). Here, we delve into the details of using the DE optimization strategy to solve the cost function illustrated in Eq. (3).

We define $\theta_{i,G}$ as the ith parameter vector in the Gth generation by:

$$\theta_{i,G} = (a_{i,G}, b_{i,G}, c_{i,G}, d_{i,G}, t_{xi,G}, t_{yi,G}, t_{zi,G}) \tag{4}$$

where $i = (1, 2, \ldots, P_{total})$, and $G = (1, 2, \ldots, G_{max})$ by assigning the size of population to $POPULATION_{total}$, and the maximum number of generations to G_{max}. We employ the mutation operator $\boldsymbol{p_{i,G}} = \theta_{p,G} + S \times (\theta_{q,G} - \theta_{r,G})$ to produce deviation from one generation of a population to the next. $S \in [0, 2]$ and $\theta_{p,G}, \theta_{q,G}, \theta_{r,G}$ are three individual random agents in the population. The DE algorithm for solving the problem in Eq. (3) is described by the following Pseudo-code:

Algorithm 1.

Algorithm 1. Proposed DE algorithm for 3D SEM surface reconstruction.

Input: Matching points, initial SEM extrinsic parameters and 3D locations.

Output: The best fitness of SEM extrinsic parameters and 3D points.

```
begin
Initialization:
read S, CR, POPULATION_Total, G_max;
Initialize the population {θ_i; (1< =i< =POPULATION_Total)}
randomly;
for (G=1; G <G_max; G ++)
for (i=1; i< =POPULATION_Total; i++)
Mutation and Crossover:
choose three individual agents θ_p,G, θ_q,G, θ_r,G randomly;
L = U(0,1);
if L < CR
p_i,G = θ_p,G + S × (θ_q,G − θ_r,G)
else
p_i,G = θ_i,G;
if p_i,G < θ_i,G;
θ* = p_i,G;
end.
end.
return θ*
end.
```

The parameters CR $\in$[0, 1] and S $\in$[0, 2] will be obtained by performing several experiments on the problem. We started with seven-dimensional parameter vector (θ^*) which is randomly assigned from the uniformly distributed numbers in the range (0, 1) at generation $G = 1$. During each generation ($G + 1$), a new parameter vector including both rotation and translation parameters was then generated by adding the weighted difference vector between two population members to a third member. After G_{max} iterations ensuring convergence ($G_{max} = 1000$ in our experiments) the population member θ^* with the highest confidence is considered to present the best solution.

As part of our future work, we will develop a set of web services as a reusable and platform independent software components to automatically perform these steps and provide 3D SEM surface reconstruction as a service. The web services will be freely available over the Internet for any educational, academic, and research purposes.

3. Experimental validations

In order to validate the general performance, accuracy, and speed of the proposed system discussed in Section 2, extensive experiments on real and also synthetic data were carried out. In Section 3.1, we first present the experimental setup by configuring the different parameters and showing data attributes. Then, in Section 3.2, we show qualitative 3D visualization results obtained from three real samples. After that, in Section 3.3, we measure and compare the accuracy of our proposed framework to SEM extrinsic calibration using the ground truth SEM rotation. In Section 3.4, we study the convergence rate of the our proposed strategy with respect to different numbers of generations employed by the DE algorithm. At the end of experimental validations, in Section 3.5 we further examine and compare the system accuracy on 3D shape modeling by applying the proposed method on a set of synthetic data.

3.1. Experimental setup

A Hitachi S-4800 field emission scanning electron microscope was used to generate the micrographs for this study. This microscope is equipped with a computer controlled 5 axis motorized stage capable of 360 degrees of rotation with a tilt range of −5

Table 3
Experimental setup. We used $G = 1000$ (stopping condition for the DE algorithm) based on the experiments illustrated in Section 3.3 to satisfy both accuracy and the time efficiency. The initial population for the parameter space (θ) was generated as uniformly distributed random numbers in the range (0, 1). The reason for choosing such a range is related to the common possible tilting angles in a SEM which is almost (0 to $\pi/4$).

Datasets	(1): *Pollen grain* from *Brassica rapa*
	(2): TEM *copper grid*
	(3): Tapetal cell of *Arabidopsis thaliana*
Images attributes	(1): 854*640 grayscale, 512 dpi
	(2) and (3): 2560*1920 grayscale, 512 dpi
SEM detector	SE (mix)
SEM intrinsic parameters	A = [0.047 0 0; 0 0.047 0; 0 0 1]
DE parameters	$CR = 0.8, S = 0.9$
	$POPULATION_{Total} = 55, G_{max} = 1000$

to 70 Å. Sample manipulation, such as tilt, Z-position, and rotation of the stage, as well as image processing and capture functions were operated through the Hitachi PC-SEM software. The working distance that would give the required depth of focus was determined at the maximum tilt for each specimen at the magnification chosen for image capture. As the sample was tilted in successive 1 Å increments through the software, the image was centered manually by moving the stage in the x- and y-axes with the stage positioning trackball. The working distance and magnification were kept consistent in each captured image of the tilt series by changing the Z-axis position as required. Brightness and contrast were manually adjusted for consistency between micrographs, using the same structure in each image. The micrographs were acquired with an accelerating voltage of 3 kV, utilizing the signals from both the upper and lower secondary electron detectors.

The proposed 3D SEM surface reconstruction system was implemented by Java2SE 7 and Matlab 2012a. We used 64-bit Windows 7 operating system on a PC with 3.00 GHz Intel Dual core CPU, 4 MB cache and 4 GB of RAM. Datasets names and attributes, SEM configurations, and initial parameters in our DE based algorithm are shown in Table 3.

3.2. Qualitative 3D visualization

Three real samples are shown in Fig. 4–6. The first rows in these figures show a set of 2D images obtained from different perspectives. Their 3D point clouds, 3D surface meshes, and 3D shape models which were reconstructed by using the proposed system are presented in the second, third, and fourth rows in each figure respectively. The 3D geometric models presented here indicate that the proposed method is promising for 3D SEM surface reconstruction. Magnified views of the reconstructed 3D surfaces are also shown in Fig. 7. By considering these results, it is evident that the larger SEM snapshots (SEM micrographs) improved the quality of the reconstruction process, although the computation time increased. Including more corresponding points and employing bigger rotation angles will also enhance the quality of the 3D reconstructed surfaces.

3.3. SEM extrinsic calibration

This section presents a validation summary on the reliability, accuracy, and time efficiency of the proposed strategy for SEM rotation estimation. We present various experimental results performed on multiple data sets including *pollen grain* from *Brassica rapa*, TEM *copper grid*, and tapetal cell of *Arabidopsis thaliana* (Figs. 4–6). We were given the rotation angles, but rotation axis and translation vector were unknown. By using only two images in each set and setting the maximum number of DE generations to 1000, we got a rotation matrix R_1 and translation vector t_1 for the *pollen*
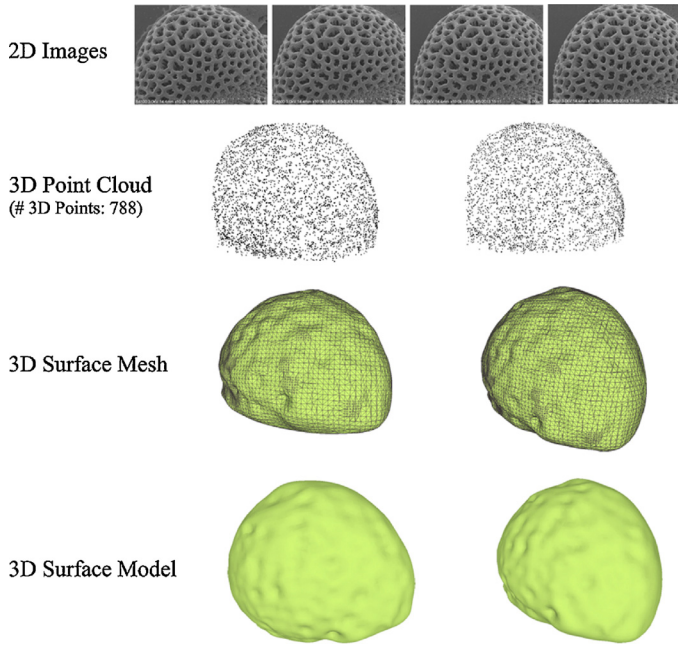
Fig. 4. Qualitative visualization of 3D SEM surface reconstruction. This figure shows 2D SEM images, 3D point clouds, 3D reconstructed surface meshes, and surface models of a *pollen grain* from *Brassica rapa*. We present 3D point clouds, 3D surface meshes and the shape models from different perspectives. 2D images were obtained by tilting the specimen stage 3 degrees from one to the next in the image sequence. The attributes of these 2D images are illustrated in Table 3. In Section 4, we also discuss about the figure in further details.
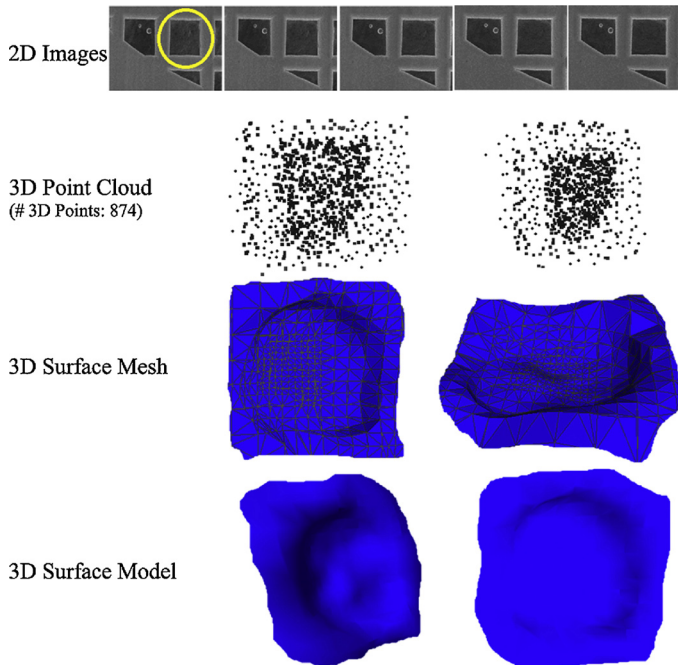

Fig. 5. Qualitative visualization of 3D SEM surface reconstruction. In this figure, we present 2D SEM images, 3D point clouds, 3D surface meshes, and 3D shape models of a part of a TEM *copper grid* which specified by the yellow circle in the first 2D image (at the first rows). We show 3D point clouds, 3D surface meshes and the shape models from different views. The 2D images were taken by tilting the TEM *copper grid* 7 degrees from one to next in the sequence. The attributes of these 2D images are presented in Table 3. We discuss about this figure in Section 4.
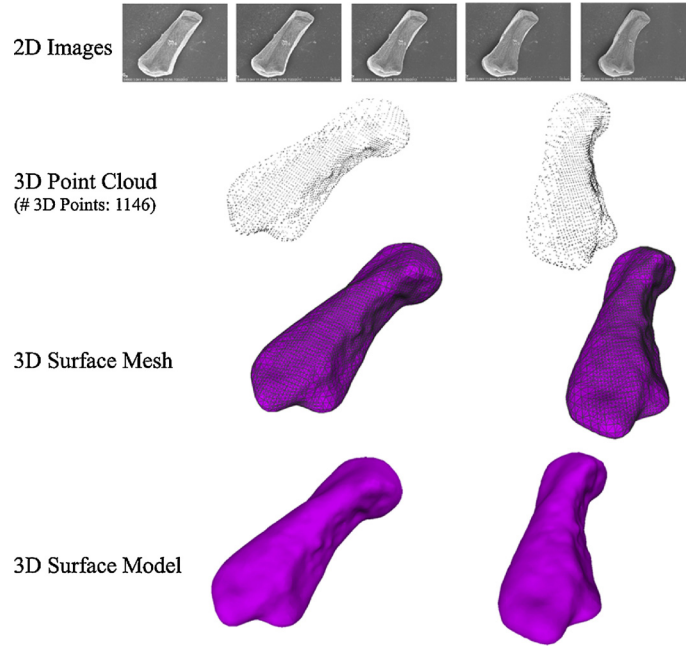

Fig. 6. Qualitative visualization of 3D SEM surface reconstruction. The figure shows 2D SEM images, 3D point clouds, 3D surface meshes, and 3D reconstructed surfaces of a *tapetal cell of Arabidopsis thaliana* from different views. These images were obtained by tilting the specimen stage 9 degrees from one to the next in the image set. The attributes of these 2D images are shown in Table 3. For further discussion please refer to Section 4.
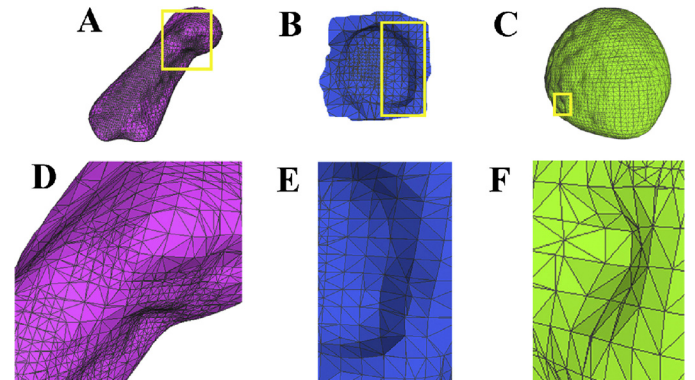

Fig. 7. A magnified view of 3D SEM surface reconstruction. (A) A 3D reconstructed surface of a *tapetal cell of Arabidopsis thaliana*. (B) A 3D shape model of a part of a TEM *copper grid*. (C) A 3D surface model of a *pollen grain* from *Brassica rapa*. (D) A close view of the yellow rectangular area in (A). (E) A close view of the yellow rectangular area in (B). (F) A close view of the yellow rectangular area in (C).

grain from *Brassica rapa* (tilting by 3 degrees), R_2 and t_2 for the TEM *copper grid* (tilting by 7 degrees), and R_3 and t_3 for the tapetal cell of *Arabidopsis thaliana* (tilting by 9 degrees) as follows:

$$R_1 = \begin{bmatrix} 1.0000 & 0.0011 & 0.0006 \\ 0.0003 & 0.9927 & -0.1515 \\ 0.0019 & 0.1515 & 0.9927 \end{bmatrix} \tag{5}$$

$$R_2 = \begin{bmatrix} 1.0000 & 0.0006 & 0.0019 \\ 0.0009 & 0.9861 & -0.1673 \\ 0.0033 & 0.1673 & 0.9861 \end{bmatrix} \tag{6}$$

$$R_3 = \begin{bmatrix} 1.0000 & 0.0005 & 0.0015 \\ 0.0007 & 0.9822 & -0.1877 \\ 0.0014 & 0.1877 & 0.9822 \end{bmatrix} \tag{7}$$

Table 4
Accuracy and reliability validation of the proposed method by examining different variables. ΔR is given as $R_{real} - R_{estimated}$, indicating error for estimating the 3D rotation. Rotation angles show the ground truth 3D SEM rotations(R_{real}). In each row we used only two images in the set.

Image set	Total matches	Rotation angle	G_{max}	ΔR	Elapsed time (s)
Pollen grain	749	3 degrees	500	4.31E−03	10.13
Pollen grain	749	3 degrees	1000	8.33E−04	12.08
Pollen grain	749	3 degrees	1250	5.57E−04	13.29
Pollen grain	673	6 degrees	500	4.72E−03	8.97
Pollen grain	673	6 degrees	1000	8.84E−04	9.62
Pollen grain	673	6 degrees	1250	6.69E−04	10.17
Pollen grain	618	9 degrees	500	8.01E−03	8.01
Pollen grain	618	9 degrees	1000	8.92E−04	9.13
Pollen grain	618	9 degrees	1250	7.11E−04	9.73
Copper grid	830	7 degrees	500	3.11E−03	14.08
Copper grid	830	7 degrees	1000	7.94E−04	15.33
Copper grid	830	7 degrees	1250	7.12E−04	16.83
Copper grid	722	14 degrees	500	4.59E−03	10.01
Copper grid	722	14 degrees	1000	8.61E−04	11.73
Copper grid	722	14 degrees	1250	7.07E−04	12.12
Copper grid	658	21 degrees	500	5.81E−03	9.83
Copper grid	658	21 degrees	1000	8.97E−04	10.77
Copper grid	658	21 degrees	1250	6.04E−04	11.91
Tapetal cell	509	9 degrees	500	2.12E−03	6.61
Tapetal cell	509	9 degrees	1000	5.07E−04	9.18
Tapetal cell	509	9 degrees	1250	5.02E−04	9.63
Tapetal cell	441	18 degrees	500	2.57E−03	6.53
Tapetal cell	441	18 degrees	1000	7.12E−04	8.89
Tapetal cell	441	18 degrees	1250	6.86E−04	9.18
Tapetal cell	413	27 degrees	500	2.89E−03	5.19
Tapetal cell	413	27 degrees	1000	7.49E−04	7.68
Tapetal cell	413	27 degrees	1250	7.11E−04	8.35

Table 5
Comparison of our proposed DE based model with two traditional approaches demonstrates that our system provides a greater improvement to the accuracy and time efficiency of SEM rotation estimation. Here, we investigate and compare our method with ADBA and ASDBA techniques. We labeled our proposed method as DE.

Method	Image set	Total matches	Rotation angle	ΔR	Elapsed time (s)
ADBA	Pollen grain	749	3 degrees	7.59E−02	21.02
ASDBA	Pollen grain	749	3 degrees	6.13E−02	19.53
DE	Pollen grain	749	3 degrees	8.33E−04	12.08
ADBA	Pollen grain	673	6 degrees	4.17E−02	20.88
ASDBA	Pollen grain	673	6 degrees	3.09E−02	19.01
DE	Pollen grain	673	6 degrees	8.84E−04	9.62
ADBA	Pollen grain	618	9 degrees	4.04E−02	19.35
ASDBA	Pollen grain	618	9 degrees	2.51E−02	18.92
DE	Pollen grain	618	9 degrees	8.92E−04	9.13
ADBA	Copper grid	830	7 degrees	3.88E−02	24.57
ASDBA	Copper grid	830	7 degrees	3.03E−02	20.16
DE	Copper grid	830	7 degrees	7.94E−04	15.33
ADBA	Copper grid	722	14 degrees	6.17E−02	20.06
ASDBA	Copper grid	722	14 degrees	4.44E−02	18.73
DE	Copper grid	722	14 degrees	8.61E−04	11.73
ADBA	Copper grid	658	21 degrees	4.66E−02	21.11
ASDBA	Copper grid	658	21 degrees	3.07E−02	17.84
DE	Copper grid	658	21 degrees	8.97E−04	10.77
ADBA	Tapetal cell	509	9 degrees	7.39E−02	21.74
ASDBA	Tapetal cell	509	9 degrees	9.86E−03	16.18
DE	Tapetal cell	509	9 degrees	5.07E−04	9.18
ADBA	Tapetal cell	441	18 degrees	2.41E−02	19.44
ASDBA	Tapetal cell	441	18 degrees	5.19E−03	15.09
DE	Tapetal cell	441	18 degrees	7.12E−04	8.89
ADBA	Tapetal cell	413	27 degrees	4.73E−02	20.35
ASDBA	Tapetal cell	413	27 degrees	5.32E−03	15.01
DE	Tapetal cell	413	27 degrees	7.49E−04	7.68

$$t_1 = [0.10073\ 0.0019\ 0.0029] \tag{8}$$

$$t_2 = [0.2164\ 0.1003\ 0.0017] \tag{9}$$

$$t_3 = [0.3727\ 0.1020\ 0.0002] \tag{10}$$

Reviewing 3D rotation matrices (Hartely and Zisserman, 2004) we can definitely claim that the rotation axis is the *X*-axis. Various analysis from different angles in images and different numbers of DE generations (G_{max}) are presented in Table 4. The 3D rotation estimation error (ΔR) ranges from 5.02E−04 to 5.81E−03, mostly depending on the G_{max}. It is evident that the reliability and the robustness of our approach remains acceptable by using different rotation angles, different images, and a varying number of matching points. We did not perform ground truth evaluation for the translation vector, as a SEM cannot supply such a predefined information on translation. However our estimation for translation values appear to have worked for 3D SEM surface reconstruction.

We have also compared the experimental results of our proposed approach with two other traditional approaches; namely algebraic distance bundle adjustment (ADBA) and adaptive sampson distance bundle adjustment (ASDBA) (Torr and Murray, 1997; Triggs et al., 2000; Albouy et al., 2004) (Table 5). Elapsed times in Tables 4 and 5 indicate only SEM extrinsic calibration. A graphical comparison of 3D reconstructed surfaces of *tapetal cell of Arabidopsis thaliana* using ADBA, ASDBA, and DE techniques is shown in Fig. 8.

3.4. Convergence rate of the proposed system

In this section we analyze the convergence rate of our proposed framework with respect to different numbers of generations (G_{max}) in Algorithm 1. The graphical comparisons for both biological samples using Algorithm 1 are presented in Fig. 9. In this experiment we only use two images tilted by 3 degrees with 749 3D points
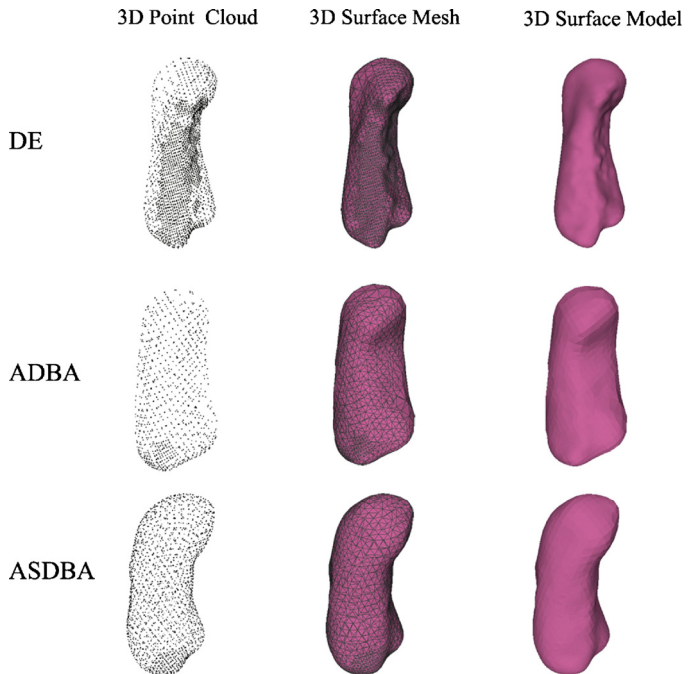

Fig. 8. A graphical comparison of 3D reconstructed surfaces of tapetal cell of *Arabidopsis thaliana* using DE, ADBA, and ASDBA techniques. We labeled our proposed method as DE. The graphical comparison shows that our proposed DE based strategy would be able to provide a better and detailed 3D surface model. Further quantitative comparisons are illustrated in Section 3.5 and Table 6.

for *pollen grain*, 7 degrees with 830 point clouds for TEM *copper grid* and 9 degrees with 509 3D points for *tapetal cell* set. The experiment clearly demonstrates that the proposed model has a stable convergence behavior with respect to the different numbers of generations and different 2D images.
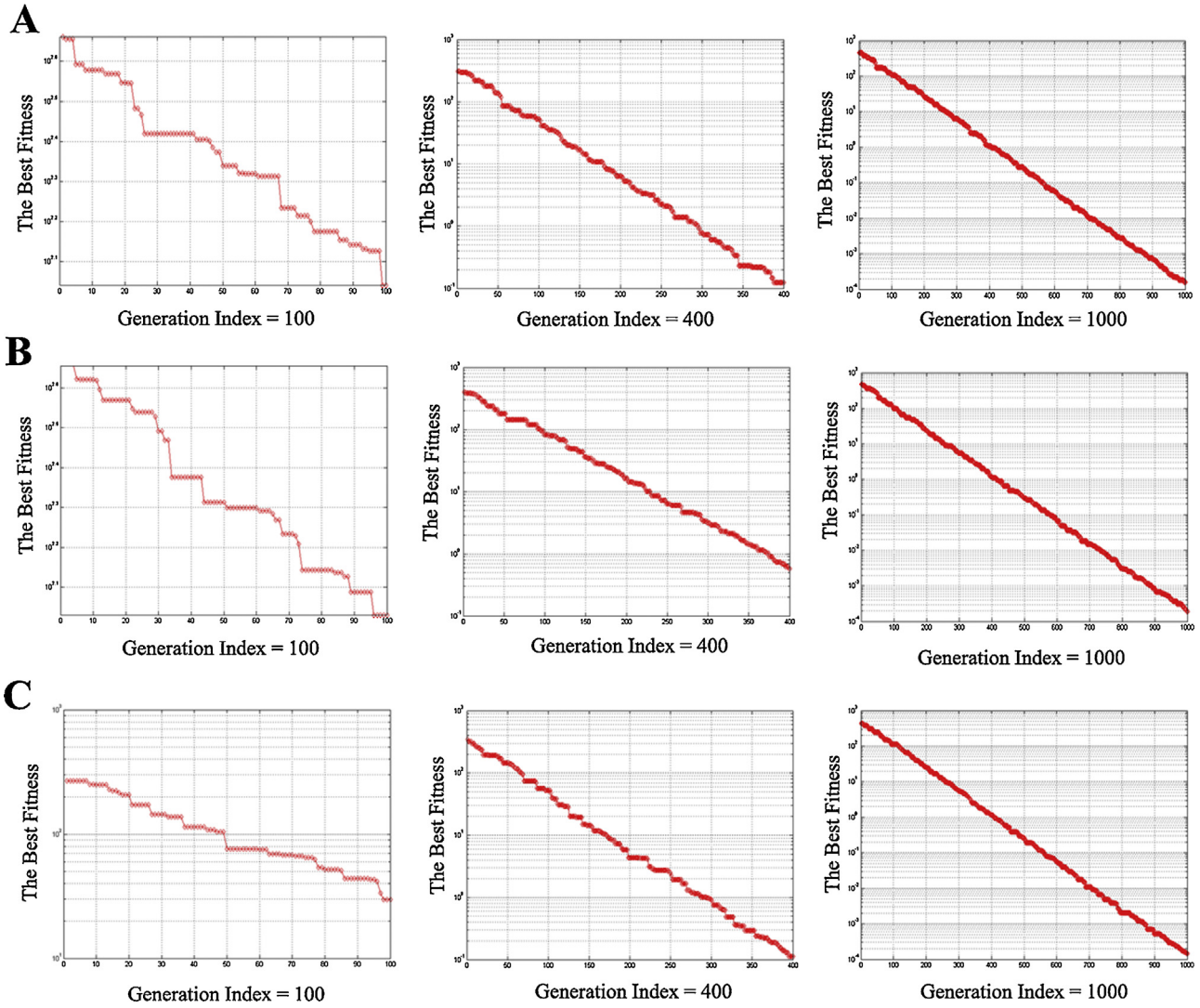
Fig. 9. The convergence rates for *Pollen grain* (first row), TEM *copper grid* (second row), and *tapetal cell* (last row) with respect to different number of generations in Algorithm 1. Horizontal and vertical axes show the generation indexes, and the best fitnesses respectively.

3.5. Quantitative comparisons of 3D SEM surface reconstruction

By applying our proposed system on synthetic 3D "*Face*" models (Paysan et al., 2009), we quantitatively compare the accuracy of the approach with traditional methods mentioned in Section 3.3. In this experiment, we compute the geometric difference between the 3D "*Face*" models using Hausdorff Distance unit (HDu) (Cignoni et al., 1998; Munkres, 1999). HDu is able to measure how close two subsets of a metric space are to each other. Minimum, maximum and mean of HDu values were computed between the original 3D "*Face*" models as a reference, with those estimated using the proposed system and also the different methods. We employed Meshlab (Meshlab, 2005) as an advanced 3D triangular mesh processing application to compute the HDu values. The mean and maximum of the HDu values which are exposed in Table 6 clearly assert that our proposed framework can produce more accurate 3D models than the other methods. Fig. 10 shows a graphical 3D reconstructed surfaces using our proposed framework.

4. Discussion

There are a number of outstanding issues with 3D SEM surface reconstruction techniques which we discuss here. We divide this

Table 6
Hausdorff Distance unit values on the synthetic "*Face*" Models. In this table, our implementation is denoted as the proposed system. The first three rows in the table show HDu values for Fig. 10(A), and the last three rows show the same for Fig. 10(B).

Method	Number of 3D points	HDu (min)	HDu (max)	HDu (mean)
ADBA	5206	0.000000	0.206809	0.110701
ASDBA	5206	0.000031	0.090974	0.008747
The proposed system	5206	0.000000	0.020917	0.003329
ADBA	4318	0.000000	0.147315	0.040482
ASDBA	4318	0.000000	0.090102	0.008093
The proposed system	4318	0.000000	0.008013	0.001605

section into two parts. In Section 4.1, we point out the problems and challenges in SEM based 3D surface reconstruction, and then, in Section 4.2, we address several insights and directions for possible future enhancements in this rapid progressing field.

4.1. Problems and challenges

In this section we further discuss the problems and challenges in 3D SEM surface reconstruction using different techniques as illustrated in the taxonomy (Fig. 2).
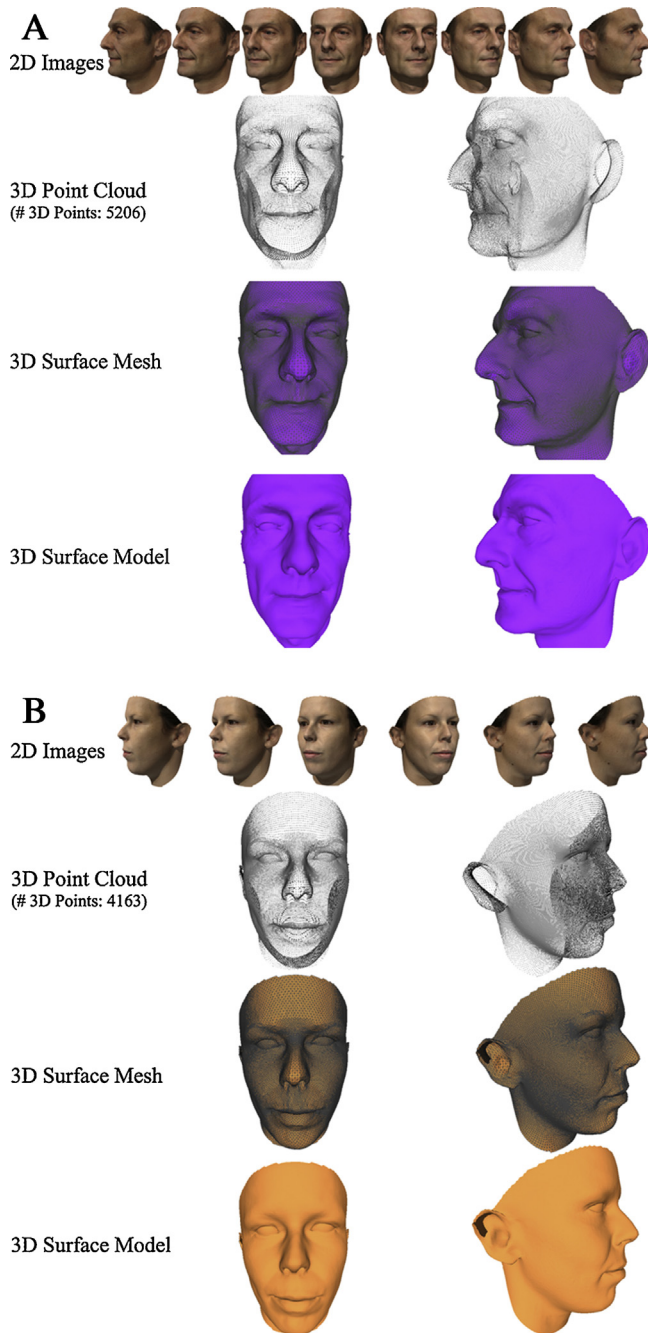
Fig. 10. Quantitative comparisons of 3D surface reconstruction. (A) A set of eight 2D images of the synthetic "*Face*" model along with its 3D point cloud and the shape structure are shown in this figure. These images were tilted 25 degrees from one to the next in the image sequence. 5206 3D points were used in the experiment to compare the accuracy on 3D shape modeling. (B) This figure shows a set of six 2D images of another synthetic "*Face*" model. The 3D point cloud and the shape structure are also shown in the figure. These images were tilted 34 degrees from one to the next in the image sequence. 4163 3D points were used in the experiment to compare the accuracy on 3D shape modeling. Comparing results for both models are exposed in Table 6.

Invisible parts will not be reconstructed The main problem is that both single-view and multi-view 3D SEM surface reconstruction algorithms are applicable for those surfaces which are completely visible in a sample. Invisible and occluded parts by other objects or components will not be restored.

Distortions and noise in SEM images Like any other microscopic devices, the SEM images are exposed to different types of errors which interferes with a pure signal. The most prominent errors include: (1) image distortions caused by the plane array of the detectors, (2) the elements of this array might have unequal sensitivity causing error, (3) also, the quadruple detector system being asymmetric generates some errors, and (4) noise as an unwanted component generated during the whole process of SEM imaging causes some errors as well (Drzazga et al., 2006).

Multiple highlights and shadows Employing BSE detectors, the SEM images will suffer from multiple highlights and shadowing effects. The presence of shadows or highlights have been responsible for reducing the reliability of 3D SEM surface reconstruction techniques, in particular for single-view approaches (Argyriou and Petrou, 2006).

Limited number of images The other problem is that we may have to reconstruct the 3D surface model from a small number of SEM images. While the accuracy of multi-view 3D SEM surface reconstruction strategies needs to take a large number of images, the SEM specimen can tilt only from −5 to at most 70 degrees, depending on the size of the specimen mount (usually diameter) that the sample is mounted on as well as the location of the specimen (Z or height) within the column of the microscope. These constraints limit the number of images may be taken. On the other hand, small rotation angle does not appear to be appropriate to restore a reliable 3D surface from 2D images. As in Fig. 4 (Section 3), using tiny rotation angle (3 degree) would produce unruffled 3D shape models. Analyzing Figs. 4–7 (Section 3), it is also evident that employing bigger rotation angles and larger SEM snapshots (SEM micrographs) improves the quality of the reconstruction process, although the computation time would increase.

Outliers Multi-view 3D SEM surface reconstruction approaches take as input multiple images and bring 3D point cloud and camera poses in a standard 3D coordinate system. The technique requires model estimation based on the detected feature points in the first stage of its pipeline (Fig. 3 in Section 2). So, the reliable detection of feature points (inlier) has a conclusive impact on the quality of 3D reconstruction and also the extrinsic calibration of the SEM machine. In other words, the outliers which come from noise or false matching points will limit the accuracy of 3D SEM surface reconstruction. The technique needs a very well-organized feature tracker which is able to detect correct corresponding points and consequently enhance the quality of the 3D reconstructed surfaces (Figs. 4–7 (Section 3)).

Vanishing points In multi-view 3D SEM surface reconstruction algorithms, one critical problem arises from vanishing points in the image sequence. Using multi-view surface reconstruction systems, we use projective geometry principal to initialize the 3D position of only matching points in the image set. As we begin considering more than two images, it becomes unlikely that all matching points in the first image pair are observable in the other pairs. The only existing way to tackle the problem is using the incremental pipeline (Klopschitz et al., 2010; Wu, 2013). The incremental multi-view 3D surface reconstruction is a iteratively growing reconstruction process in which it starts from an initial two-view reconstruction, and then iteratively extended by adding new views and 3D points, using both pose estimation and triangulation. The technique was employed as part of our proposed framework in Section 2.

No practical/operational datasets are available Highly operational and public datasets for SEM images are not available now on the Internet. To further examine and analyze the quality attributes of the 3D SEM surface reconstruction algorithms such as accuracy, reliability, robustness, and efficiency, we need to access a variety of SEM images by employing different light directions (single-view) or different points of view (multi-view).

4.2. Possible future enhancements

Here, we point out different future enhancements which may affect the research in several ways.

Low-level and medium-level image processing techniques In the previous section we mentioned several sources in the SEM in which they produce different kinds of noises, highlights and multiple shadows on SEM images which consequently decrease the reliability and accuracy of 3D SEM surface modeling. Digital image processing techniques are widely used in such areas due to their ability to reduce noises (Shao et al., 2014), detect shadows (Kersten et al., 1997) and highlights and remove them from the original images. One future enhancement is to create a system that can automatically perform low and medium level image processing algorithms to provide better 2D images such that they can help us to produce much more reliable 3D surfaces.

Adaptive approaches One of the challenges we discussed earlier was the presence of outliers which have been one of the causes for reducing the quality of 3D SEM surface reconstruction and its extrinsic calibration. Since every SEM images has its own properties (i.e. contrast, illumination, darkness, brightness, etc.), we propose to apply a statistical model estimation algorithm which enables us to control the number of true and false detections based on the image attributes. This strategy yields validation thresholds automatically adapted to the complexity of the feature point detector to be matched with the diversity of image properties.

Application area The value of any research might be evaluated by how effective it is in real applications. We introduced several applications of the 3D SEM surface reconstruction in Section 1. A desirable improvement would be expanding the application areas from bioscience, material, and mechanical engineering to other scientific domains which need to know and evaluate the 3D shape information. The present work is expected to stimulate more interest and draw attentions from the computer vision community to the fast-growing SEM application area.

Public datasets Recovering the structures of SEM images requires to have a database which includes a bunch of different SEM images under the variety of light directions as well as different perspectives. We foresee a need to extend such a public and global database over the Internet to examine and analyze the 3D SEM surface reconstruction methods by applying them to various microscopic samples and SEM images.

3D microscopy avatars Creating 3D avatars is one of the keystones of many computer vision, computer graphic, and computer-aided design applications (Lee et al., 2004, 2005; Kurillo et al., in press; Kokane et al., 2014). 3D microscopy avatars can be used in Apps, distance teaching and learning, video games, interactive books, 3D printing, and anywhere we want a 3D version of a real microscopic object.

Machine learning community There is not yet a principal computation innovation based on the machine learning approaches. We believe that some novel solutions are beyond the scope of computer vision and require collaboration from the machine learning and artificial intelligence community. The resulting algorithms will allow researchers to achieve higher accuracy with limited computational complexity, and make the approaches appropriate for real-time operations.

Embedded system architecture community As we discussed in Section 1, 3D SEM surface reconstruction makes a great success in a variety of applications. However, its extensive computational complexity has been a problem to implement such a real-time system. Considering hardware issues along with effective embedded system design (Qiu et al., 2009; Zhong et al., 2013) will reduce the time complexity and it would be able to provide real-time 3D microscopy vision.

Software architecture and Internet of things community As an important enhancement, it is beneficial to design, develop and implement a set of web services as the reusable, platform independent, and extensible software components for 3D SEM vision to allow application-to-application interaction over the standard Internet protocols. These web services will provide a distributed platform to create communication between the highly demand computer vision applications and World Wide Web services, open the doors from the 3D microscopy vision to the Internet of Things (IoT) area.

Plug 3D SEM into cloud Cloud computing is one of the most discussed topics in the computer science world in recent years. Today, people choose cloud applications in such a case where they have more integrity as well as low-cost implementations. On the other hand, several big software companies have started the development of cloud services to explore the benefits of incorporating such cloud architecture services in their own business. As the number of Cloud computing services are increasing rapidly, the essential need for such a particular framework appears. Plugging 3D SEM surface reconstruction into Cloud would take full advantages of Cloud computing by deploying 3D microscopy vision as a service in private Clouds with Amazon or Google for vastly expanding research, academic and educational purposes.

References

Agarwal, S., Furukawa, Y., Snavely, N., Simon, I., Curless, B., Seitz, S.M., Szeliski, R., 2011. Building Rome in a day. Commun. ACM 54 (10), 105–112.

Albouy, B., Treuillet, S., Lucas, Y., Birov, D., 2004. Fundamental matrix estimation revisited through a global 3D reconstruction framework. In: Advanced Concepts for Intelligent Vision Systems.

Altman, N.S., 1992. An introduction to kernel and nearest-neighbor nonparametric regression. Am. Stat. 46, 175–185.

Argyriou, V., Petrou, M., 2006. Recursive photometric stereo when multiple shadows and highlights are presents. In: In: IEEE Conference on Computer Vision and Pattern Recognition.

Bay, H., Tuytelaars, T., Gool, L.V., 2006. Speeded up robust features. In: In: European Conference of Computer Vision (ECCV), Graz, Austria.

Bay, H., Ess, A., Tuytelaars, T., Gool, L.V., 2008. Surf: speed up robust features. Comput. Vis. Image Underst. 110, 346–359.

Bogner, A., Jouneau, P.H., Thollet, G., Basset, D., Gauthier, C., 2007. A history of scanning electron microscopy developments: towards wet-stem imaging. Micron 38, 390–401.

Bozzola, J.J., Russel, L.D., 1992. Electron Microscopy. Jones and Bartlett, USA.

Calonder, M., Lepetit, V., Strecha, C., Fua, P., 2010. Brief: Binary Robust Independent Elementary Features. Springer, ECCV.

Carli, L., Genta, G., Cantatore, A., Barbato, G., Chiffre, L.D., Levi, R., 2011. Uncertainty evaluation for three-dimensional scanning electron microscope reconstructions based on the stereo-pair technique. Meas. Sci. Technol. 22 (3), 035103.

Cazaux, J., 2005. Recent developments and new strategies in scanning electron microscopy. J. Microsc. 217, 16–35.

Chakraborty, U.K., 2008. Advances in Differential Evolution. Prentice Hall, USA.

Chandler, D.E., Robertson, R.W., 2009. Bioimaging: Current Concepts in Light and Electron Microscopy. Jones and Bartlett, USA.

Chen, D., Miyamoto, A., Kaneko, S., 2012. Robust surface reconstruction in SEM with two BSE detectors. In: In: Mechatronics REM.

Cignoni, P., Rocchini, C., Scopigno, R., 1998. Metro, measuring error on simplified surfaces. Comput. Graph. Forum 17, 167–174.

Cornille, N., Garcia, D., Sutton, M., McNeill, S., 2003. Automated 3D reconstruction using a scanning electron microscope. In: In: SEM Annual Conference and Exposition on Experimental and Applied Mechanics.

Crandall, D., Owens, A., Snavely, N., Huttenlocher, D., 2011. Discrete-continuous optimization for large-scale structure from motion. In: In: CVPR 2011.

Cyganek, B., Siebert, J.P., 2009. An Introduction to 3D Computer Vision Techniques and Algorithms. Wiley, UK.

Danzl, R., Scherer, S., 2003. Integrating shape from shading and shape from stereo for variable reflectance surface reconstruction from SEM images. In: In: SEM Images, 26th Workshop of the Austrian Association for Pattern Recognition.

Drzazga, W., Paluszynski, J., Slowko, W., 2006. Three-dimensional characterization of microstructures in a SEM. Meas. Sci. Technol. 17, 28–31.

Egerton, R., 2005. Physical Principles of Electron Microscopy: An Introduction to TEM, SEM, and AEM. Springer, USA.

Estellers, V., Thiran, J.-P., Gabrani, M., 2014. Surface reconstruction from microscopic images in optical lithography. IEEE Trans. Image Process. 23 (8), 3560–3573.

Feoktistov, V., 2006. Differential Evolution. Springer, Germany.

Fischler, M.A., Bolles, R.C., 1981. Random sample consensus: a paradigm for model fitting with applications to image analysis and automated cartography. Commun. ACM.

Fridman, K., Mader, A., Zwerger, M., Elia, N., Medalia, O., 2012. Advances in tomography: probing the molecular architecture of cells. Nat. Rev. Mol. Cell Biol., 736–742.

Ghosh, A., Mondal, A., Ghosh, S., 2014. Moving object detection using Markov random field and distributed differential evolution. Appl. Soft Comput. 15, 121–136.

Hartely, R., Zisserman, A., 2004. Multiple View Geometry in Computer Vision. Cambridge University Press, UK.

Hayakawa, H., 1994. Photometric stereo under a light source with arbitrary motion. J. Opt. Soc. Am., 3079–3089.

Hobrough, L.G., 1957. Methods and Apparatus for Correlating Corresponding Points in Two Images (US67997857A).

Horn, B.K.P., 2012. Shape from Shading: A Method for Obtaining the Shape of a Smooth Opaque Object From One View, Technical Report. MIT.

Ikeuchi, K., Horn, B.K.P., 1981. Numerical shape from shading and occluding boundaries. Artif. Intell.

Kersten, D., Mamassian, P., Knill, D.C., 1997. Moving cast shadows induce apparent motion in depth. Perception 26, 171–192.

Kirkpatrick, S., Gelatt, C.D., Vecchi, M.P., 1983. Optimization by simulated annealing. Science 220, 671–680.

Kizilyaprak, C., Daraspe, J., Humbel, B.M., 2014. Focused ion beam scanning electron microscopy in biology. J. Microsc., 109–114.

Klopschitz, M., Irschara, A., Reitmayr, G., Schmalstieg, D., 2010. Robust incremental structure from motion. In: In: Fifth International Symposium on 3D Data Processing, Visualization and Transmission (3DPVT).

Kodama, T., Li, X., Nakahira, K., Ito, D., 2005. Evolutionary computation applied to the reconstruction of 3-D surface topography in the SEM. J. Electron Microsc. 54 (5), 429–435.

Kokane, A., Singhal, H., Mukherjee, S., Reddy, G.R., 2014. Effective e-learning using 3D virtual tutors and WebRTC based multimedia chat. In: In: International Conference on Recent Trends in Information Technology (ICRTIT), Chennai, India.

Kozera, R., Noakes, L., 1999. A 2D lead-frog algorithm for optimal surface reconstruction. In: In: Proc SPIE99, Vision Geometry VIII-3811.

Kozera, R., Cameron, T., Datta, A., 2006. A parallel leap-frog algorithm for 3-source photometric stereo. In: In: Computational Imaging and Vision, ICCVG'04.

Kurillo, J., Koritnik, T., Bajd, T., Bajcsy, R., 2011. Real-time 3D avatars for tele-rehabilitation in virtual reality. In: Medicine Meets Virtual Reality. NextMed.

Lazaros, N., Sirakoulis, G.C., Gasteratos, A., 2008. Review of stereo vision algorithms: from software to hardware. Int. J. Optomech. 2, 435–462.

Lee, S.-Y., Kim, I.-J., Ahn, S.C., Ko, H., Lim, M.-T., Kim, H.-G., 2004. Real time 3D avatar for interactive mixed reality. In: In: Proceedings of the 2004 ACM SIGGRAPH International Conference on Virtual Reality Continuum and Its Applications in Industry (VRCAI '04), New York, USA.

Lee, S.-Y., Kim, I.-J., Ahn, S.C., Lim, M.-T., Kim, H.-G., 2005. Toward immersive telecommunication: 3D video avatar with physical interaction. In: In: Proceedings of the 2005 International Conference on Augmented Tele-existence (ICAT '05), New York, USA.

Longuet-Higgins, H., 1981. A computer algorithm for reconstructing a scene from two projections. Nature 293 (10), 133–135.

Lowe, D.G., 2004. Distinctive image features from scale-invariant keypoints. Int. J. Comput. Vis. 60 (2), 91–110.

Li, Y., Snavely, N., Huttenlocher, D., Fua, P., 2012. Worldwide pose estimation using 3D point clouds. In: In: ECCV.

Liu, X., Hu, H., Jiang, W., Sun, X., 2012. Object-oriented modified photometric stereo algorithm for 3D imaging in fiber-to-chip coupling. In: In: IEEE 9th International Conference on Group IV Photonics (GFP).

Lourakis, M.A., Argyros, A., 2009. SBA: a software package for generic sparse bundle adjustment. ACM Trans. Math. Softw. 36 (1), 1–30.

Marinello, F., Bariani, P., Savio, E., Horsewell, A., Chiffre, L.D., 2008. Critical factors in SEM 3D stereo microscopy. Meas. Sci. Technol. 19 (6), 065705.

Meshlab, 2005. http://meshlab.sourceforge.net/.

2005. Mex Software. Alicona Imaging GmbH, Graz, Austria.

Munkres, James R., 1999. Topology. Prentice Hall, USA.

Nyirarugira, C., Taeyong, K., 2013. Adaptive differential evolution algorithm for real time object tracking. IEEE Trans. Consum. Electron., 59.

Okabe, A., Boots, B., Sugihara, K., Chiu, S.N., 2000. Spatial Tessellations: Concepts and Applications of Voronoi Diagram. Wiley, USA.

Paluszynski, J., Slowko, W., 2005. Surface reconstruction with the photometric method in SEM. Vaccum 78, 533–537.

Parry-Vernon, K.D., 2000. Scanning electron microscopy: an introduction. III-Vs Rev. 13, 40–44.

Paysan, P., Knothe, R., Amberg, B., Romdhani, S., Vetter, T., 2009. A 3D face model for pose and illumination invariant face recognition. In: In: Proceedings of the 6th IEEE International Conference on Advanced Video and Signal based Surveillance (AVSS) for Security, Safety and Monitoring in Smart Environments, Genova, Italy.

Pintus, P., Podda, S., Vanzi, M., 2006. An automatic alignment procedure for a 4-source photometric stereo technique applied to scanning electron microscopy. In: In: IMTC – Instrumentation and Measurement, pp. 989–996.

Qiu, J., Huang, T., Ikenaga, T., 2009. A FPGA-based dual-pixel processing pipelined hardware accelerator for feature point detection in sift. In: In: International Joint Conference on INC, IMS, and IDC, pp. 1668–1675.

Raspanti, M., Binaghi, E., Gallo, I., Manelli, A., 2005. A vision-based 3D reconstruction techniques for scanning electron microscopy: direct comparison with atomic force microscopy. Microsc. Res. Tech. 67, 1–7.

Rittscher, J., Machiraju, R., Wong, S.T.C., 2008. Microscopic Image Analysis for Life Science and Applications. Artech House, USA.

Roberts, L., (PhD Thesis) 1963. Machine Perception of Three-Dimensional Solids. MIT.

Rousseeuw, P., 1984. Least median of squares regression. J. Am. Stat. Assoc. 79, 871–880.

Rublee, E., 2011. ORB: an efficient alternative to sift or surf. In: In: IEEE International Conference on Computer Vision.

Samak, D., Fischer, A., Rittel, D., 2007. 3D reconstruction and visualization of microstructure surfaces from 2D images. Ann. CIRP 56, 149–152.

Shao, L., Yan, R., Li, X., Liu, Y., 2014. From heuristic optimization to dictionary learning: a review and comprehensive comparison of image denoising algorithms. IEEE Trans. Cybern., 1001–1013.

Shotton, J., Fitzgibbon, A., Cook, M., Sharp, T., Finocchio, M., Moore, R., Kipman, A., Blake, A., 2011. Real-time human pose recognition in parts from a single depth image. In: In: CVPR 2011.

Slowko, W., Krysztof, M., 2013. Detector system for three-dimensional imaging in the variable pressure/environmental SEM. In: In: IX International Conference on ION.

Snavely, N., Seitz, S.M., Szeliski, R., 2008. Modeling the world from internet photo collections. Int. J. Comput. Vis. 80, 189–210.

Tafti, A.P., Hassannia, H., Yu, Z., 2015. siftservice.comturning a computer vision algorithm into a world wide web service, arXiv preprint arXiv:1504.02840.

Tafti, A.P., Hassannia, H., Borji, A., Yu, Z., 2015. Computer vision as a service: towards an easy-to-use platform for computer vision researchers. In: In: CVPR 2015: Vision Industry and Entrepreneur Workshop (VIEW 2015).

Tomasi, C., Kanade, T., 1990. Shape and motion without depth. In: In: Proceedings of the Third International Conference in Computer Vision, pp. 91–95.

Torr, P., 2002. Bayesian model estimation and selection for epipolar geometry and generic manifold fitting. Int. J. Comput. Vis. 50, 35–61.

Torr, P.H.S., Murray, D.W., 1997. The development and comparison of robust methods for estimating the fundamental matrix. Int. J. Comput. Vis. 24, 271–300.

Triggs, B., McLauchlan, P.F., Hartley, R., Fitzgibbon, A.W., 2000. Bundle adjustment a modern synthesis. Vis. Algorithms: Theory Pract. 1883, 298–372.

Vynnyk, T., Schultheis, T., Fahlbusch, T., Reithmeier, E., 2010. 3D-measurement with the stereo scanning electron microscope on sub-micrometer structures. J. Eur. Opt. Soc. Rapid Publ. 5.

Warren, J.S., 2007. Modern Optical Engineering. McGraw-Hill, USA.

Wohler, C., 2013. 3D Computer Vision Efficient Methods and Applications. Springer, Germany.

Woodham, R., 1980. Photometric method for determining surface orientation from multiple images. Opt. Eng. 19, 139–144.

Wu, C., 2013. Towards linear-time incremental structure from motion. In: International Conference on 3D Vision (3DV).

Yuniarti, A., 2007. 3D Surface Reconstruction of Noisy Photometric Stereo. University of Western Australia.

Zhao, W., 2011. A Comprehensive Study Over Flip Invariant SIFT, Technical Report.

Zhong, S., Wang, J., Yan, L., Kang, L., Cao, Z., 2013. A real-time embedded architecture for sift. J. Syst. Archit. 59, 16–29.

Zickler, T., Belhumeur, P.N., Kriegman, D.J., 2002. Helmholtz stereopsis: exploiting reciprocity for surface reconstruction. Int. J. Comput. Vis. 49, 215–227.

Zolotukhin, A., Safonov, I., Kryzhanovskii, K., 2013. 3D reconstruction for a scanning electron microscope. Pattern Recognit. Image Anal. 23 (1), 168–174.